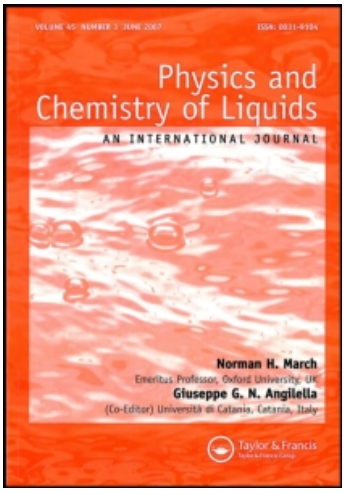

Physics and Chemistry of Liquids
Publication details, including instructions for authors and subscription information:
http://www.informaworld.com/smpp/title~content=t713646857

Many-Body Effects in the Static Structure of Dense Krypton and Xenon

J. Youden[a]; P. A. Egelstaff[a]
[a] Guelph-Waterloo Program for Graduate Work in Physics, University of Guelph, Ontario, Canada

To cite this Article Youden, J. and Egelstaff, P. A.(1994) 'Many-Body Effects in the Static Structure of Dense Krypton and Xenon', Physics and Chemistry of Liquids, 28: 2, 79 — 94
To link to this Article: DOI: 10.1080/00319109408029545
URL: http://dx.doi.org/10.1080/00319109408029545

Phys. Chem. Liq., 1994, Vol. 28, pp. 79–94
Reprints available directly from the publisher
Photocopying permitted by license only

MANY-BODY EFFECTS IN THE STATIC STRUCTURE OF DENSE KRYPTON AND XENON

J. YOUDEN and P. A. EGELSTAFF

Guelph-Waterloo Program for Graduate Work in Physics, University of Guelph, Guelph, Ontario N1G 2W1, Canada

(Received 30 November 1993)

The effects of many-body interactions in the static structure of dense gaseous krypton (for 0.9–2.1 ρ_c, where ρ_c is the critical density) and xenon (for 2.2–2.6 ρ_c) were investigated in the momentum transfer range $4 \leqslant Q \leqslant 42\,\mathrm{nm}^{-1}$, through comparisons of the measured structure factors $S(Q)$ with those calculated through the MHNC-CRS integral equation by Reatto and Tau[1]. One property investigated is the small increase in the effective atomic diameter with increasing density[2]. While the observed variation, as determined through the position of the main diffraction maxima, is similar to that given by the inclusion of the Axilrod-Teller[3] triple–diploe interaction in the calculation, further small deviations exist which indicate the need for additional many-body terms.

KEY WORDS: Neutron scattering, structure of fluids, interatomic interactions.

1 INTRODUCTION

Whereas at low densities the properties of a fluid may be derived from the pair interaction alone, at higher densities the influence of so-called higher order interactions, that arise due to the atomic polarizability, can be significant. The effects of these many-body interactions in dense fluids have been investigated already through various macroscopic thermodynamic and transport properties, as well as in the microscopic dynamic and static structure (see, for example, Egelstaff, 1988; and the references therein). The dynamic and static structure for a fluid of number density ρ, may be described either through the position r and time t dependent pair correlation functions $G(r,t)$ and $\rho g(r) = G(r, t = 0)$, or through their Fourier transforms which are the corresponding momentum Q and energy ω dependent structure factors $S(Q,\omega)$ and $S(Q)$. These functions provide an opportunity to examine the many-body effects in detail, since the r, t or equivalently Q, ω dependences of the interactions are included explicitly. For simple fluids, extensive studies of these functions have already been made, for example, for fluid krypton at a number of states[4–7]. Recently, Tau *et al.*[8] (1989) have reviewed the experimental data on the static structure of krypton in order to re-examine the many-body effects. In this paper we shall discuss the static structure only.

While the most important many-body term in the interaction potential is usually assumed to be the Axilrod–Teller[3] triple–dipole interaction, a number of previous experimental measurements have illustrated that additional terms contribute to the structure—either from short or intermediate range three-body forces, or higher-order

interactions. One such term is the short-range, exchange three-body interaction (see, for example, Loubeyre[9,10]). However, compared to the experimentally observed many-body effects in the static structure, the inclusion of this extra term appears to have minimal effect[8], and whereas the exchange term is attractive overall agreement with the experimental data would require a repulsive contribution. Thus, although the discrepancies that exist between the experimental and the Axilrod–Teller many-body contributions have often been attributed to shorter range interactions, the exact nature of these terms remains to be determined. Furthermore, the multipole expansion up to the triple quadrupole has been considered also, and it fails to account for the observed many-body effects[8].

One topic of interest here is the possibility of an observable increase in the effective atomic diameter with increasing density (e.g. Egelstaff[2] who used older published data on $S(Q)$ for krypton and xenon gases and preliminary theoretical predictions). Although this behaviour has been a given simple physical interpretation in terms of collision diameters the magnitude of the observed change was uncertain due to the large errors on the experimental and theoretical data available. It is worth noting that a similar effect has been calculated for a simple one-dimensional quanum mechanical model (Nickel[11]), and it can be associated also with the Axilrod–Teller interaction. Therefore, more accurate experiments and calculations, especially at high densities, are required to take this study further.

The present $S(Q)$ measurements were designed to examine the possible change in the effective atomic diameter with density, and to provide $S(Q)$ measurements at high densities for further investigation of the many-body terms. Thus, the structure factors $S(Q)$ in the Q range of 4–45 nm^{-1} were determined through neutron diffraction measurements, for krypton and xenon at room temperature, within the density ranges of 6–14 nm^{-3} (0.9–2.1 ρ_c, where ρ_c is the critical density) for krypton and 11–13 nm^{-3}(2.2–2.6 ρ_c) for xenon. Due to its relatively large size and polarizability, xenon gas is particularly appropriate for this study although its nuclear parameters are unfavourable. The measurements for krypton provided further tests of the many-body contributions, in a range of reduced densities just below that for xenon, and also permitted a check of the previous approximate data as obtained by Egelstaff *et al.*[15] through integration of measured $S(Q,\omega)$ spectra. The nuclear parameters for natural krypton are unfavourable also, and the advantages of working with the isotope ^{86}Kr will be pointed out.

The experimental data will be compared to structure factors calculated by Reatto and Tau[12] using the modified hypernetted chain (MHNC) integral equation with the cross-over bridge function (CRS). The overall accuracy of this integral equation has been verified against computer simulation data to be at least 1% (Tau *et al.*[8]; and the references therein), but the accuracy at specific conditions is not known precisely. They calculated the structure factor due to the pair interaction alone using the accurate pair potential of Aziz[13], while further calculations with the addition of the Axilrod–Teller interaction permitted the effect of this three-body term to be examined. In an attempt to reduce the systematic errors due to errors in the nuclear data we shall fit our data to the theoretical MHNC curves at low and high values of Q for one of our states. Thus the differences we report are the irreducible

minimum differences. Because of the importance, to this field, of accurate data we shall describe our procedures in full.

2 DIFFRACTOMETER

The experiments on fluid krypton and xenon were carried out on the University of Guelph diffractometer[14] at the NRU Reactor, Chalk River. Neutrons of wavelength 0.240 nm were incident on the sample, and the relative neutron intensity was measured by a fission chamber placed at the position of a beam defining slit in the incident beam. The scattered neutrons were then detected by three arrays of ^{3}He proportional counters (σ_a(He) = 7111 bns for 0.24 nm neutrons). The detectors were located 2.16 m from the sample centre, on a platform that rotated in 0.5° angular steps through the range from about 0 to 120°. These positions were calibrated against the known Bragg reflections of polycrystalline samples, such as lead and copper. The detectors were either rectangular with width 38 mm and height 0.36 m, or cylindrical with diameter 12 mm and height 0.15 m or with diameter 25 mm and height 0.41 m; and had efficiencies for 0.24 nm neutrons of 95% and 75% for the two thicker types respectively. The first array contained two of the smaller cylindrical detectors installed for specific use in the low angle region. The intermediate angle array consisted of five rectangular detectors, while the high angle array used three pairs of the larger cylindrical type. These three arrays covered the respective momentum transfer regions of less than 26 nm^{-1}, 3–29 nm^{-1}, and 24–45 nm^{-1}.

The samples and their containers were housed in an aluminum cylinder, 0.45 m in diameter, that was flushed with natural argon gas in order to reduce the extraneous scattering in the vicinity of the sample. A cadmium vane could be positionsed just after the sample chamber to absorb the transmitted neutron beam, and hence reduce the scattering by the air in the flight path to the detectors. Alternatively, with this vane removed the transmission of any particular sample could be determined using a second fission chamber in conjuction with the incident beam monitor. The size of the neutron beam incident on the sample was 12.7 × 50.5 mm and the alignment between the centre of the slit and the axis of the cylindrical sample deviated by 0.3 mm during these measurements, as determined using neutron camera photographs. Extra cadmium shielding was attached directly to the sample support so that only scattering in the angular range from 0 to 130° could escape into the detectors. Over the duration of the experiments, the positioning of the sample was checked periodically using additional neutron photographs.

The procedure for data collection consisted of recording, during the dwell time at each angular position, the number of events recorded by each detector over the time period ($\sim$ 180s) required for 10^6 monitor counts in the first fission chamber. For the present set of experiments as many as sixteen scans were taken for each sample, thereby ensuring a statistical accuracy of much better than 1% in the final structure factor. During the experiment, the data from the various scans for a given sample were checked for self consistency to ensure that any systematic fluctuations were within the desired accuracy of 1%. Longer term stability was investigated by comparing sets of

data—for the titanium cell or the vanadium rod—which were taken before and after measurements on the fluid samples.

Samples

For the investigation of the static structure of dense krypton and xenon, five room temperature states were chosen for each gas—see Table 1—where for krypton they covered the density range from 6–14 nm^{-3} (0.9–2.1 ρ_c) and for xenon the range was 11–13 nm^{-3}(2.2–2.6 ρ_c). Smaller steps in density were used for xenon than krypton for reasons of convenience. Thus, for these samples—with an average path length of 18.9 mm—the resulting fraction of the incident neutrons that were scattered varied respectively from 8–18% and 8–10%. In terms of the *L-J* well depth parameters for these gases the temperature in Table 1 is about 1.8ε and 1.3ε respectively. The sample absorption was large, varying from 32 to 59% and 48 to 55% for the krypton and xenon samples respectively.

A titanium-alloy cylindrical container with an inside diameter of 20.32 mm and a wall thickness of 3.31 mm was used to confine the gaseous samples. The cell was pressure tested to 204 MPa without any discernable deformation. The coherent scattering and absorption cross sections for the alloy were calculated using a weighted average over the cross sections of the elemental components. The incoherent scattering cross section was determined by first calculating the average, mean and mean-squared scattering lengths for the particular alloy composition. Approximately 12% of the incident neutrons were scattered by the container, with the incoherent scattering comprising 70% of this amount.

Some high density sample states were obtained using a high pressure gas handling system which incorporated a cryopump that was rated for pressures up to 83 MPa. To obtain the higher density states, first the sample container was cooled to a temperature of 195 K by immersing it in a dry ice and ethanol bath, and then the cryopump system was used to compress the cooled sample to the desired density, as determined from the PVT data of Streett and Staveley[15] for krypton, and Streett *et al.*[16] for xenon.

Table 1 The thermodynamic states of the krypton and xenon samples.

Element	T^a (K)	P (MPa)	ρ^b (nm^{-3})	$S(0)^c$
Krypton	296.3 ± 0.4	96.88(14)	13.985(5)	0.147
Krypton	295.5 ± 0.2	58.13(14)	12.125(5)	0.275
Krypton	299.4 ± 0.4	36.97(3)	10.045(5)	0.530
Krypton	297.8 ± 0.3	24.84(3)	8.019(8)	0.968
Krypton	295.4 ± 0.5	17.73(3)	6.05(1)	1.463
Xenon	296.6 ± 0.2	132.07(14)	13.130(2)	0.062
Xenon	296.6 ± 0.2	118.18(34)	12.897(6)	0.068
Xenon	295.7 ± 0.4	105.83(17)	12.698(3)	0.074
Xenon	298.5 ± 0.7	74.34(21)	11.998(5)	0.102
Xenon	299.2 ± 0.3	42.82(3)	11.000(2)	0.169

[a] The variations in the temperature result from the fluctuations in the temperature of the room.
[b] The uncertainty in the density is that associated with the uncertainty in the measured pressure.
[c] For Xe, $S(0)$ was calculated for T= 298 K.

Finally, the liquid sample was closed off from the rest of the system and warmed to room temperature.

The pressures below 68 MPa were measured with a pressure transducer, while for the higher pressures a 0–200 MPa Bourdon tube gauge was used. Both of these gauges were calibrated using a precision dead weight balance (Whalley and McLaren[17]). The Bourdon gauge possessed a small hysteresis effect, however over the high pressure range where it was used the slope of the density versus pressure curve was small, and accurate determinations of the density could be achieved (see data in Table 1). The sample temperature was monitored with two platinum resistance temperature detectors. Since no active temperature control was used, the fluctuations were generally around ± 0.3 K, with occasional deviations of as high as 0.7 K. The sample densities were calculated from the measured PT data using published PVT curves. The compilation by Rabinovich *et al.*[18] provided equations of state for both krypton and xenon; however their validity is restricted to densities below $2\rho_c$. Thus, the values for the higher densities relied on the original data at 298 K of Trappeniers *et al.*[19] for krypton, and Michels *et al.*[20] for xenon.

The absolute normalization of all sets of data was based on the incoherent scattering from a 6.478 mm diameter vanadium rod, which was completely immersed in the incident neutron beam. Hence an accurate determination could be made of the total number of atoms that contributed to the scattering, and the attenuation factors were not particularly sensitive to the exact location of the rod with respect to the centre of the beam. In addition to the above, various other measurements were required to evaluate the background contributions. The room background was measured with a cadmium absorber located in front of the sample. To isolate the background associated with the main neutron beam, extra measurements were made with an empty sample environment, as well as on two different cadmium cylinders with diameters corresponding to those of the sample container and the vanadium rod. These data were used in a conventional way[21].

4 DATA ANALYSIS

The starting point in an analysis of neutron data, is a table of neutron cross sections [eg. Mughabghab *et al.*[22] or Sears[23]]. We used these two tables for the cross sections of our titanium alloy, and we used Dilg[24] for the cross sections of vanadium. However for krypton there is a discrepancy between the two tables[22,23] which we feel may be due to an error in the Sears[23] table (a new experimental result is given in the appendix). For krypton and xenon, the cross sections used and their references are given in Table 2. Slight variations in σ_a for krypton and σ_c for xenon will be made in the normalization procedure described later, which was used to reduce the error in the ratio of $\sigma_c/\sigma_s = \gamma$.

The procedure for obtaining the static structure factor $S(Q)$ from neutron diffraction data has been given in numerous previous papers (see, for example, Egelstaff[21], and the references therein). The approach used here was similar to that of Teitsma and Egelstaff[4]. For the lower angles of the intermediate array a small adjustment was applied to the nominal angle to account for the average angle of the scattering cone

Table 2 Cross Sections for Krypon and Xenon.

Element	*Bound Scattering* σ_s *(barns)*	*Coherent Scattering* σ_a *(barns)*	*Ratio* γ	*Nuclear Absorption* σ_a *(barns) at* 1.8 A
Kr	[a] 7.79 ± 0.04	[b] 7.21 ± 0.15	0.93 ± 0.02	[b] 25 ± 1
Xe	[a] 4.36 ± 0.02	[c] 2.96 ± 0.16	0.68 ± 0.04	[c] 23.9 ± 1.2

[a] from Krohn & Ringo[24].
[b] from Mughabghab *et al.*[22]
[c] from Sears[23].

that was incident on the linear detectors. For the detectors of this array, from their lower angular limit of 7° ($3\,\mathrm{nm}^{-1}$) up 22° ($10\,\mathrm{nm}^{-1}$), this adjustment varied from $0.2\,\mathrm{nm}^{-1}$ to $0.05\,\mathrm{nm}^{-1}$. For each detector and angular position, the data from the various scans for a particular sample were checked for consistency then added together to give the total intensity $I_i(\theta)$ along with the associated statistical standard deviations, where here the subscript i refers to one of the thirteen detectors used. These quantities were then normalized to the total intensity of the incident beam monitor.

After the above corrections have been applied, the intensity I_{sc} for scattering from N_s sample atoms and N_c container atoms can be written as

$$I_{sc}(\theta) = \frac{1}{K(\theta)} N_s A_{s,sc}(\theta) \langle b_s^2 \rangle \{\gamma_s [S_s(\theta) - 1] + [1 + P_s(\theta) + \Delta_{sc}(\theta)]\}$$

$$+ \frac{1}{K(\theta)} N_c A_{c,sc}(\theta) \langle b_c^2 \rangle \{\gamma_c [S_c(\theta) - 1] + [1 + P_c(\theta) + \Delta_{sc}(\theta)]\}$$

Here, the subscripts s, c refer to the sample and container respectively; $A_{i,jk}(\theta)$ is the attenuation factor for scattering from medium i and attenuation in media j and k; $\Delta(\theta)$ is the ratio of multiple to single scattering; $P(\theta)$ is the inelasticity correction; $K(\theta)$ is the normalization factor. The mean-square scattering length is denoted by $\langle b^2 \rangle$, and by γ the ratio $\langle b \rangle^2 / \langle b^2 \rangle$. Similarly, the respective intensities for the scattering from N_c container atoms and N_v vanadium atoms are

$$I_c(\theta) = \frac{1}{K(\theta)} N_c A_{c,c}(\theta) \langle b_c^2 \rangle \{\gamma_c [S_c(\theta) - 1] + [1 + P_c(\theta) + \Delta_c(\theta)]\}, \tag{2}$$

$$I_v(\theta) = \frac{1}{K(\theta)} N_v A_{v,v}(\theta) b_{i_v}^2 [1 + P_v(\theta) + \Delta_v(\theta)], \tag{3}$$

where the latter expression is used to define the normalization factor $K(\theta)$ in terms of the incoherent scattering from vanadium. The values of N_c and A_c were calculated by folding the neutron beam profile with the sample geometry. The static structure factor $S(Q)$ is obtained by combining these three equations for the experimental neutron spectra to give

$$a\left\{[S_s(\theta) - 1]\frac{\gamma_s}{F_{sc}(\theta)} + 1\right\} = \left[I_{sc}(\theta) - I_c(\theta)\frac{A_{c,sc}(\theta)}{A_{c,c}(\theta)}\right] \frac{N_v A_{v,v}(\theta) b_{i_v}^2 F_v(\theta)}{N_s A_{s,sc}(\theta) \langle b_s^2 \rangle F_{sc}(\theta) I_v(\theta)}, \tag{4}$$

where the correction factors F_v and F_{sc} are

$$F_v(\theta) = 1 + P_v(\theta) + \Delta_v(\theta), \tag{5}$$

$$F_{sc}(\theta) = 1 + P_s(\theta) + \Delta_{sc}(\theta) + \frac{N_c A_{c,sc}(\theta)\langle b_c^2\rangle}{N_s A_{s,sc}(\theta)\langle b_s^2\rangle}[\Delta_{sc}(\theta) - \Delta_c(\theta)]. \tag{6}$$

The factor a has been introduced to permit an adjustment (at a later stage) in the absolute value of the detector normalization, which may be necessary due to the uncertainties in the cross sections and the number of atoms in the beam.

In the above analysis, the small dependence of the coherent neutron cross section on the angle of scattering (see, for example, Foldy[25]; Squires[26]) was included for the atoms of krypton and xenon, in which case

$$\sigma_c = 4\pi(b_{n_c}^2 + 2b_{n_c}b_e F(\theta) + b_e^2 F^2(\theta)) \tag{7}$$

where b_{n_c} and b_e are defined respectively as the coherent neutron–nuclear and the neutron electron scattering lengths, and $F(\theta)$ is the atomic form factor, normalized to the atomic number. The form factor data of Hubbell *et al.*[27] was used along with the relevant scattering lengths (Krohn and Ringo[24]) to evaluate Eq. 7 over the angular range from 0 to 120°, which for krypton and xenon, resulted in respective variations of 0.5% and 1%. A further correction for the scattering of neutrons by the air in the flight path to the detectors, which decreases the amplitude of the measured structure factor by about 1%, was accounted for using the estimate of Teitsma[28].

The multiple scattering contribution was evaluated according to the method of Soper and Egelstaff[29], using the computer program MULSCA[30]. It used the isotropic approximation for the first scattering event, and the primary and secondary scattering are calculated for a sample partially immersed in an incident neutron beam of nonuniform profile. In the present case, the measured profile was approximated by a trapezoid, (with the central uniform portion comprising 83% of the total width (13.7 mm) of the beam, and offset from the axis of the cylindrical sample by 0.3 mm, away from the side on which the detectors scanned). Once the ratio of secondary to primary scattering was determined, the approximation of Sears[23] was used to estimate the higher orders of scattering, and hence the ratio of multiple to single scattering $\Delta(\theta)$. The resulting values were generally in the range of 0.12–0.14, although for some krypton samples they ranged up to 0.17.

The required attenuation factors $A_{s,s}$, $A_{s,sc}$, $A_{c,sc}$, $A_{c,c}$ and $A_{v,v}$, were calculated using the program CORKI[30], where, as in the calculation of the multiple scattering, the incident neutron beam profile was taken into account. For the higher density samples the ratio $A_{c,sc}/A_{c,c}$, which appears in the subtraction of the container scattering, varied by almost a factor of two over the angular range of 0 to 120° due to the large absorption cross sections. Since the published neutron cross sections generally have an uncertainty of several percent, the attenuation within each sample was checked by comparing the calculated and measured transmissions. The systematic variations on successive experimental measurements was about 0.3%, and a discrepancy of around 1% was found with the calculated value. The small deviations between the two

transmissions varied linearly with the density, and were therefore attributed to an error in the Kr cross section. To eliminate this discrepancy we decreased slightly the absorption cross section for krypton. This decrease in the value listed in Table 2 was bn (to 24 bn at 1.8 nm), which is also the standard error usually associated with the latter.

The inelasticity correction[21], to first order in the ratio m_n/M, of the neutron mass to the atomic mass, where $\omega_0^2 = k_B T Q^2/MS(Q)$, is

$$P(\theta) = \frac{m_n}{M}\left[\frac{k_B T}{2\hbar\omega_0}(1 - 2y + 4Ay - 2By) - 2y(1 + A)\right] \tag{8}$$

where $y = (1 - \cos\theta)/2$. The detector constants A and B are expressed in terms of the detector efficiency ε_0 for neutrons of energy corresponding to the incident energy. For vanadium at room temperature, the correction $P(\theta)$ varies from 0.018 at $\theta = 0$ to -0.054 at $\theta = 120°$, while for the heavier atoms of krypton and xenon there is a corresponding decrease in the magnitude of $P(\theta)$, and it is relatively unimportant due to the high mass M.

The static structure factors, along with the associated statistical errors, were calculated from the data for each of the ten detectors used. The momentum transfer interval for the 0.5° angular steps varies from 0.23 to 0.12 nm^{-1} over the range from 3 to 45 nm^{-1}. To convert the experimental $S(Q)$ to a 0.2 nm^{-1} uniform grid, each datum was reevaluated at the nearest 0.2 nm^{-1} grid point using a four-point Lagrangian interpolation. The data from the detectors within each of the three arrays could then be averaged together, with a corresponding reduction in the statistical errors. A weighted average over the $S(Q)$ from each array yielded the final result, along with an estimate of the statistical errors. In the latter averaging procedure, the statistical weights for the three arrays were generally about 0.08, 0.52, and 0.40, respectively.

5 RESULTS

The experimental $S(Q)$ results for the krypton and xenon samples are illustrated in Figures 1 and 2. The range of Q for which valid data were obtained was from 4.4 to 42.0 nm^{-1}, although within this range there were four regions (the blanks in the figures) in which Bragg scattering from the titanium-alloy container prevented $S(Q)$ from being determined. The statistical standard deviations are generally around 0.002 to 0.004 for the krypton data, and around 0.005 to 0.007 for the xenon data, however, the systematic uncertainty due to the errors in Table 2 is significantly larger. Although a precise estimate is difficult to make, it is of the order of 0.02 and a simple method was used to reduce this uncertainty by normalizing the data to the theoretical results. Two major uncertainties arose from the large absorption cross sections of these two samples and from the scattering by the high pressure container which was about the same size as that from the sample. Uncertainties in these quantities are manifested through the corresponding attenuation factors (see Eq. (4)), and therefore errors in the neutron cross sections (Table 2) could lead to distortions of the results for $S(Q)$.

Consequently the experimental results were normalized to the predicted $S(Q)$ at low and high Q by adjusting the nuclear parameters. In this respect our comparisons

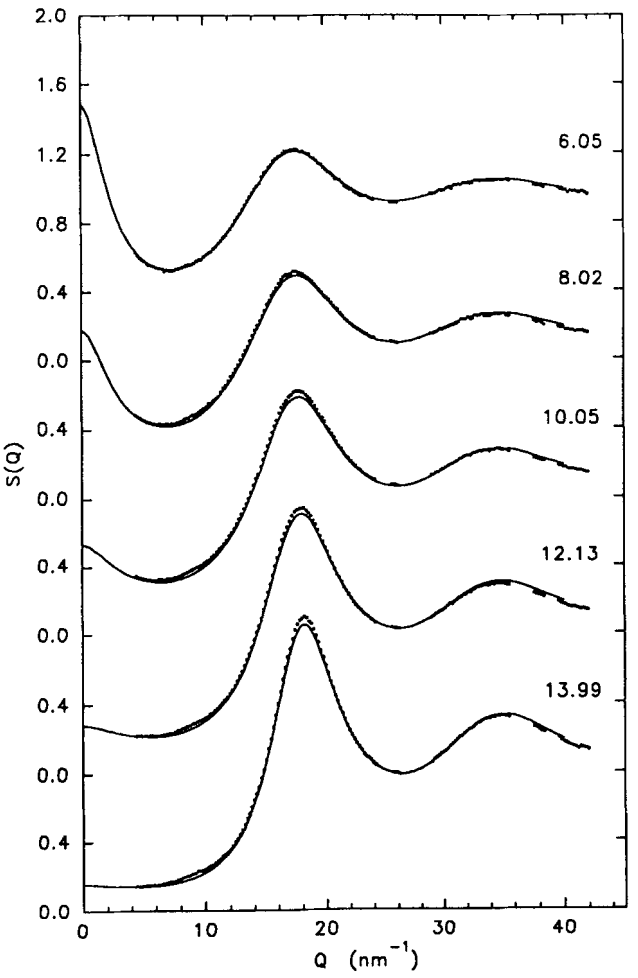

Figure 1 The experimental $S(Q)$ for the five states of krypton, (the densities in nm^{-3} are indicated on the right). Also shown are the corresponding $S(Q)$ (solid curves) as calculated from the MHNC-CRS integral equation by Reatto and Tau, (1991), using the Aziz pair potential and the Axilrod–Teller triple–dipole term.

between theory and experiment will differ from some other experimental data. The $Q \to 0$ limit is given by the compressibility equation as $S(0) = \rho k_B T \chi_T$: where ρ is the number density, and χ_T is the isothermal compressibility. Since the MHNC data fitted this limit we fitted our $S(Q)$ to the MHNC data for Q near our lower limit of $4\,nm^{-1}$(see Figures 1 and 2), at the higher densities only where $S(Q)$ varies slowly. This constraint (at the higher densities) determined the ratio of the coherent to total scattering or γ. For krypton γ was found to be 0.93, which agrees with Table 2 (also see the experimental check described in the Appendix). We note that it differs from the value of 0.95 given by Krohn and Ringo (1973) by less than half their estimated error. For xenon, the result $\gamma = 0.67$ was found, which corresponds to using $\sigma_c = 2.89$ bns in place of the value of 2.96 in Table 2 or about half the error. We shall discuss the $S(Q)$ data assuming that these values of γ have negligible error.

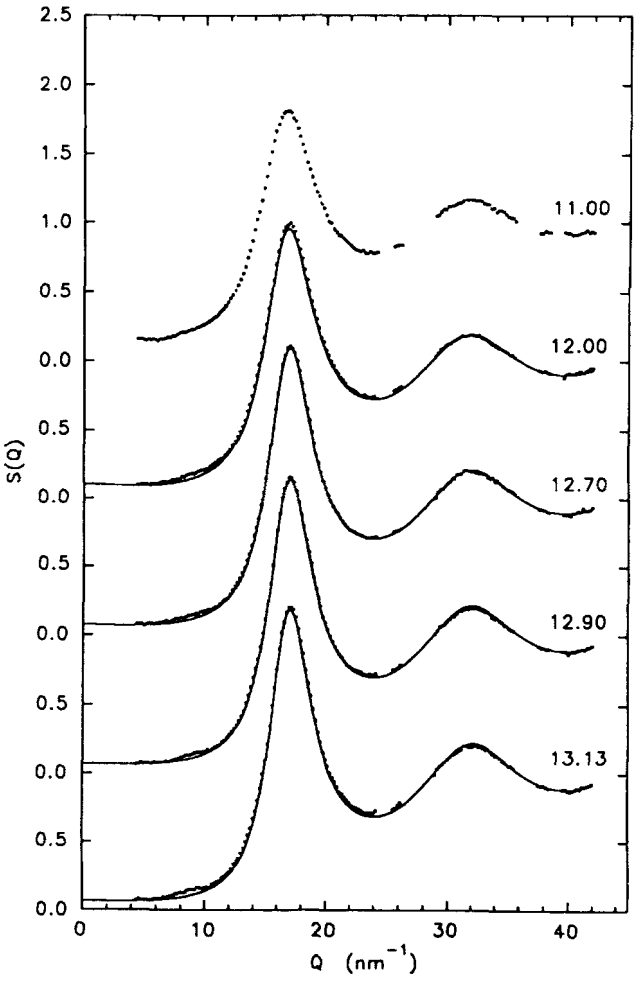

Figure 2 The experimental $S(Q)$ for the five states of xenon (the densities in nm^{-3} are indicated on the right). Also shown are the corresponding $S(Q)$ (solid curves) as calculated from the MHNC-CRS integral equation by Reatto and Tau, (1991), using the Aziz pair potential and the Axilrod–Teller triple–dipole term.

The normalization adjustment factor (a) introduced at Eq. (4) was used to correct small deviations in $S(Q)$ from its asymptotic level of unity. For the xenon samples a was set equal to 1, whereas for krypton $a = 1.015$ was required, except for the lowest density of $6.05\,nm^{-3}$ where $a = 1$ was used. These results for $S(Q)$ are tabulated by Youden[32].

6 DISCUSSION

Figures 1 and 2 contain a comparison of the experimental $S(Q)$'s for krypton and xenon to the corresponding $S(Q)$'s as calculated from the MHNC-CRS equation by Reatto and Tau[12], using both the Aziz pair potential and the Axilrod–Teller

triple–dipole potential. The overall agreement is good. Outside of the experimental errors and the accuracy of the numerical calculation, any differences between the respective structure factors are due to the effect of many-body forces beyond the triple–dipole term. For krypton, in the region of intermediate to low Q the experimental data are slightly higher than the MHNC data, and in the high Q limit the experimental data is consistently lower. Possibly a slight Q-dependence persists in the normalization of the experimental $S(Q)$ for this case. The comparisons for xenon contain smaller discrepancies between the two sets of data in the intermediate to low Q region. However in both cases at Q values around 8 to 10 nm^{-1} the experimental and theoretical data disagree by a significant amount, and it should be noted that these differences have been minimized by our normalization procedures.

The small shifts in the positions of the diffraction maxima that exist between the experimental and the MHNC $S(Q)$'s, are best examined through the differences $\Delta S(Q)$ between these sets of data. For xenon at the four highest densities, MHNC-CRS calculations were performed by Reatto and Tau[12] using the Aziz pair potential alone, as well with the Axilrod–Teller potential and therefore one may examine the effect on the structure of both the Axilrod–Teller interaction and the total many body forces in the real fluid. Figure 3 illustrates these differences where we plot points with error bars, for the highest density of xenon at $\rho = 13.13\,nm^{-3}$, and we set $\Delta S(Q) = S_e(Q) - S_{MHNC_p}(Q)$, and $\Delta S(Q) = S_{MHNC_{p,t}}(Q) - S_{MHNC_p}(Q)$, where the subscripts e and $MHNC_p$ and $MHNC_{p,t}$, respectively denote the experimental and MHNC data, with p and t designating the use of the pair and the triple–dipole potentials in the MHNC calculation. From the differences in the two MHNC calculated structures, it is evident that the triple–dipole interaction has a significant influence at low Q-below that accessible in the present experiments. However, within

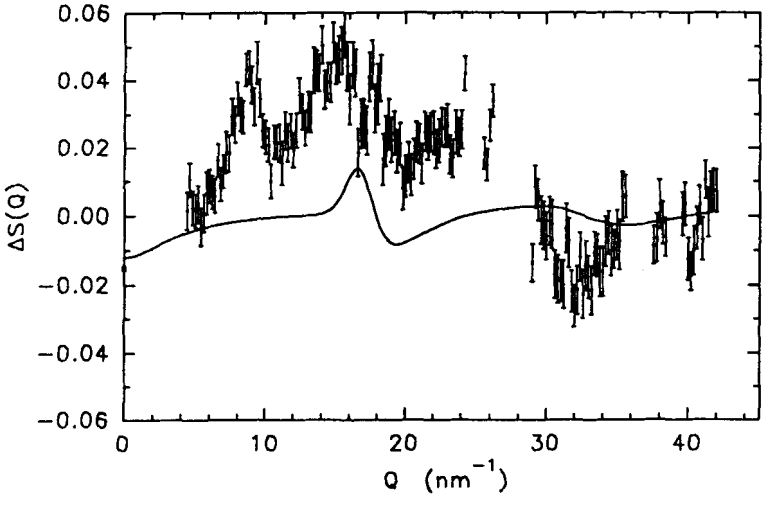

Figure 3 The effect of many body forces on $S(Q)$—for xenon at at a density of 13.13 nm^{-3}—as illustrated by the differences $\Delta S(Q) = S_e(Q) - S_{MHNC_p}(Q)$ (points with error bars), and $\Delta S(Q) = S_{MHNC_{p,t}}(Q) - S_{MHNC_p}(Q)$ (solid curve). $S_e(0)$ was obtained from the equation of state of Michels *et al.* (1954).

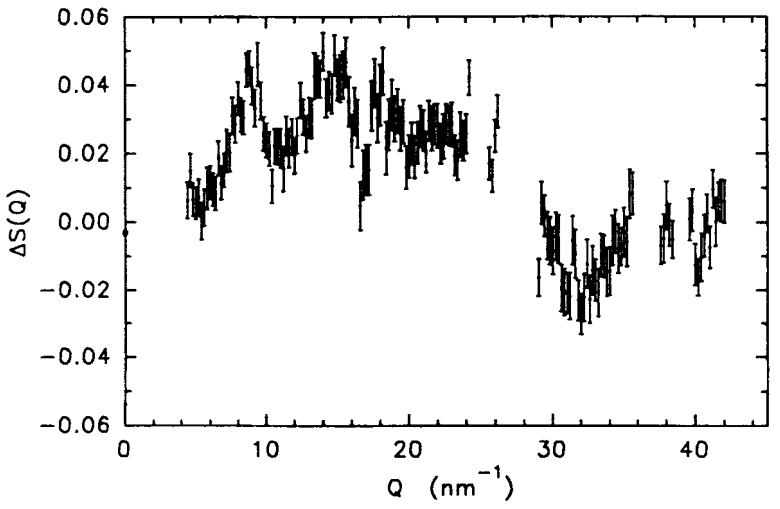

Figure 4 The contribution to the experimental structure beyond that calculated from both the pair plus triple–dipole interactions, as illustrated by $\Delta S(Q) = S_e(Q) - S_{\mathrm{MHNC}_{p,t}}(Q)$—for xenon at a density of 13.13 nm^{-3}. $S_e(0)$ was obtained from the equation of state of Michels *et al.* (1954).

the higher Q region that has been measured here, there is a slight shift in the position of the main diffraction maximum to lower Q values. Such a shift is also seen in the experimental data, although the magnitude is slightly greater. In addition, the experimental data contain a higher intensity in the intermediate Q region between approximately 5 to 20 nm^{-1}. Results for the other densities shown in Table 1 are similar to Figure 3 (Youden[32]).

Another interesting comparison is between S_e and $S_{\mathrm{MHNC}_{p,t}}$, and the difference between these two functions is shown in Figure 4 for xenon at 13.13 nm^{-3}. It may be seen that it has qualitatively the same shape as the function plotted in Figure 3. Similar plots have been made for the other densities and the variations among the data for the four densities give some indication of the effect of systematic errors. It was found that they affect slightly the amplitude and overall normalization of $S(Q)$, so that the position and width of the first maximum is relatively unaffected by these uncertainties. Throughout the analysis of the expeimental data, during which the effect of various attenuation factors on the structure was examined, the overall consistency of the first diffraction maximum with that given by the pair plus triple–dipole interactions was evident.

The structure factors for krypton as obtained from Monte Carlo simulations using the pair potential of Barker *et al.*[33] were available from Ram and Egelstaff[34]. Using these results, it was evident[32] that at high density both the real krypton fluid and that calculated though the pair and the triple-dipole interactions contain a shift of the main diffraction maximum to lower Q, similar to that exhibited in Figure 3. As well, some higher intensity of the experimental $S(Q)$ in the range of 5–20 nm^{-1}, was observed (Figure 1). Direct comparisons between the experimental $S(Q)$ for krypton and that calculated from the pair plus triple–dipole interactions, as given by the

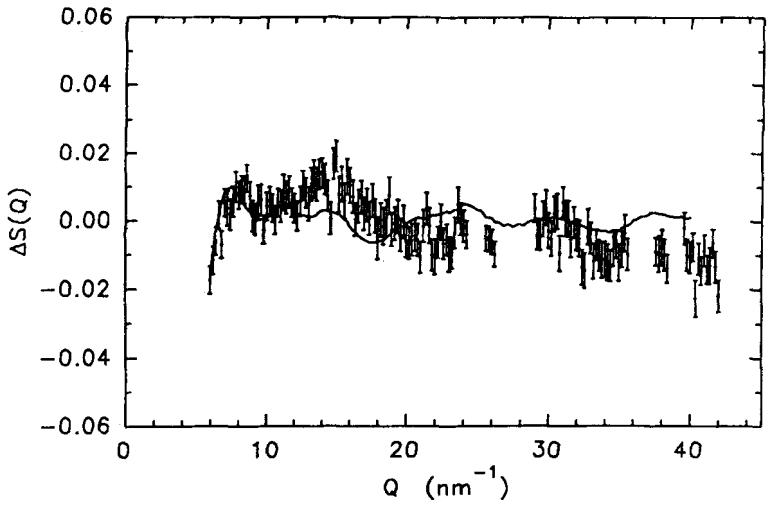

Figure 5 The contribution to $S(Q)$ beyond that simulated from the pair interaction alone, as illustrated by the differences $\Delta S(Q) = S_e(Q) - S_{MC_p}(Q)$ (points with error bars), and $\Delta S(Q) = S_{MHNC_{p,t}}(Q) - S_{MC_p}(Q)$ (solid curve), for krypton at a density of 6.05 nm^{-3}. The fluctuations in the Fourier transform of the MC data produce oscillations of magnitude ~ 0.01, throughout both difference functions.

differences $\Delta S(Q) = S_e(Q) - S_{MHNC_{p,t}}(Q)$, are shown in Figure 5 for the lowest density of 6.05 nm^{-3}. At the low density the agreement is better than at high density. In the vicinity of the first diffraction maximum, the experimental data appear to have a slightly greater intensity. This particular deviation increases with increasing density,

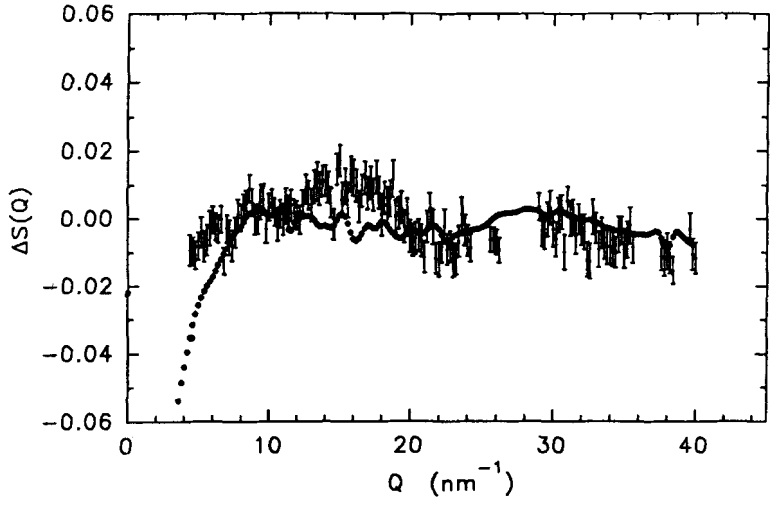

Figure 6 The contribution to the experimental structure beyond that calculated from both the pair plus triple–dipole interactions, as illustrated by $\Delta S(Q) = S_e(Q) - S_{MHNC_{p,t}}(Q)$—for krypton at a density of 6.05 nm^{-3}. The circles represent the experimental data of reference 4.

being especially evident at the higher densities (see Figure 1). Thus the real, dense fluid is characterized by slightly stronger nearest-neighbour correlations.

The differences $\Delta S(Q) = S_e(Q) - S_{\mathrm{MHNC}_{\rho,t}}(Q)$, are shown in Figure 6 for $\rho = 6.05\,\mathrm{nm}^{-3}$. Slightly higher intensity in the vicinity of the main diffraction maximum is observed and we note that the overal appearance of the curve is similar to Figure 5. The differences evaluated with the data of Teitsma and Egelstaff[4] were found to be similar to the present experimental data over most of the range. Figures showing difference functions for all the cases presented at Figure 1 may be found in Youden[32], and are qualitatively similar to Figures 3–6.

The present experimental data thus illustrate that the effects of the many-body interactions on the main diffraction maximum of the structure factor of dense noble gases, at least up to densities of $2.2\,\rho_c$, are consistent overall with that given by the Axilrod–Teller triple-dipole interaction; though the experimental $S(Q)$ exhibit slightly higher intensity in the region 5–20 nm^{-1}, implying stronger corrections on a length scale equal to or greater than the interatomic distance. In addition the variation of effective atomic diameter with density is similar in theory and experiment. In order to improve the quality of the experimental data it is necessary to use isotopically pure samples for which the nuclear absorption is negligible and $\gamma \approx 1$ (the most suitable candidate is ^{86}Kr considering both its nuclear properties and availability.) This would allow the systematic uncertainties to be reduced, and hence enable a more complete interpretation of the many-body effects.

7 CONCLUSION

The present experimental data, Figures 1 and 2, illustrate that the effects of the many body interactions on the main diffraction maximum of the structure factor of dense noble gases, at least up to densities of $2.2\,\rho_c$, are consistent overall with that given by the Axilrod–Teller interaction. In addition a slightly higher intensity of the experimental $S(Q)$ was observed in the region 5–20 nm^{-1}. Additional information on the many body interactions may be obtained be examining the $Q < 5\,\mathrm{nm}^{-1}$ region, but this was not possible using the present results. A limitation to the present experiments was the high absorption and the uncertainty in the nuclear parameter γ. Both of these difficulties may be eliminated by using separated isotopic samples (e.g. ^{86}Kr) and we propose to do this in future.

Acknowledgements

We wish to thank the staff at the NRU reactor and the Neutron and Soild State Physics Branch of A.E.C.L. Chalk River for their assistance during these neutron scattering measurements, and we gladly acknowledge the financial support of the Natural Sciences & Engineering Research Council of Canada. Also we are grateful to Drs. L. Reatto and M. Tau for tables of $S(Q)$ calculated by the MHNC-CRS theory.

References

1. L. Reatto and M. Tau, *J. Chem. Phys.* **86**, 6474 (1987).
2. P. A. Egelstaff, Can. *J. Chem.* **66**, 598 (1988).

3. B. M. Axilrod and E. Teller, *J. Chem. Phys.* **11**, 299 (1943).
4. A. Teitsma and P. A. Egelstaff, *Phys. Rev.* A **21**, 367 (1980).
5. P. A. Egelstaff, W. Glaser, D. Litchinsky, E. Schneider, and J.-B. Suck, *Phys. Rev.* A **27**, 1106 (1983).
6. H. Fredrikze, *Phys. Rev.* A **36**, 2272 (1987).
7. F. Barocchi, D. Chieux, R. Magli, L. Reatto and M. Tau, *J. Phys. Cond. Matt.* **5**, 4229 (1993).
8. M. Tau, L. Reatto, R. Magli, P. A. Egelstaff and F. Barocchi, *J. Phys. Condens. Matter* **1**, 7131 (1989).
9. P. Loubeyre, *Phys. Rev. Lett.* **58**, 1857 (1987).
10. P. Loubeyre, *Phys. Rev.* B **37**, 5432 (1988).
11. B. Nickel (Unpublished) (1987).
12. L. Reatto and M. Tau, Private communication (1991).
13. R. A. Aziz, in *Inert Gases*, ed. M. L. Klein, Springer-Verlag, Berlin (1984).
14. P. A. Egelstaff, in Faraday Discussions of the Chemical Society of London **66**, 7 (1978).
15. W. B. Street and L. A. K. Staveley, *J. Chem. Phys.* **55**, 2495 (1971).
16. W. B. Street, L. S. Sagan and L. A. K. Staveley, *J. Chem. Thermodyn.* **5**, 633 (1973).
17. E. Whalley and G. McLaren, Private communication (1989).
18. V. A. Rabinovich, A. A. Vasserman, V. I. Nedostup and L. S. Veksler, *Thermophysical Properties of Neon, Argon, Krypton and Xenon*, Hemisphere, Washington (1988).
19. N. J. Trappeniers, T. Wassenaar and G. J. Wolkers, *Physica* **32**, 1503 (1966).
20. A. Michels, T. Wassenaar and P. Louwerse, *Physica* **20**, 99 (1954).
21. P. A. Egelstaff, in *Neutron Scattering*, vol. 2, ed. K. Skold and D. L. Price, Academic Press, New York (1978).
22. S. F. Mughabghab, M. Divadeenam and N. E. Holden, Neutron Cross Sections Vol. 1, Pt. A, Academic Press N.Y. (1981).
23. V. F. Sears, *Adv. Phys.* **24**, 1 (1975) and *Neutron News* **3**(3), 26 (1992).
24. V. E. Krohn and G. R. Ringo, *Phys. Rev.* **148**, 1303 (1966).
25. L. L. Foldy, *Rev. Mod. Phys.* **30**, 471 (1958).
26. G. L. Squires, *Introduction to the Theory of Thermal Neutron Scattering*, Cambridge University Press, Cambridge (1978).
27. J. H. Hubbell, W. J. Veigele, E. A. Briggs, R. T. Brown, D. T. Cromer and R. J. Howerton, *J. Phys. Chem. Ref. Data* **4**, 471 (1975).
28. A. Teitsma, *Nuc. Instr. Meth.* **174**, 325 (1980).
29. A. K. Soper and P. A. Egelstaff, *Nuc. Instr. Meth.* **178**, 415 (1980).
30. A. K. Soper, Private communication (1986).
31. V. E. Krohn and G. R. Ringo, *Phys. Rev.* D **8**, 1305 (1973).
32. J. Youden, Ph.D. Thesis, University of Guelph (1992).
33. J. A. Barker, R. O. Watts, J. K. Lee, T. P. Schafer, and Y. T. Lee, *J. Chem. Phys.* **61**, 3081 (1974).
34. J. Ram and P. A. Egelstaff, *Phys. Chem. Liq.* **14**, 29 (1984).
35. J. Youden, P. A. Egelstaff, J. Mutka and J.-B. Suck, *J. Phys. Condens. Matter* **4**, 8945 (1992).

APPENDIX

A krypton gas sample at a temperature of 298 K and a density of 11.54 atoms/nm^{-3} was used in the experimental arrangement described by Youden *et al.*[35] in order to measure inelastic neutron scattering spectra. The containment vessel had sapphire windows which gave very little scattering, and the experimental procedure and data analysis followed that described by Youden *et al.*[35].

Examples of the results are shown in Figure A1, compared to theoretical predictions in which the ratio $\gamma = \sigma_c/\sigma_s$ was chosen to be 0.93 (i.e. the value used in section 5). At the low values of Q employed here the incoherent scattering contributes mainly to the quasi-elastic peak with a width related to the self-diffusion constant, and the coherent scattering may be calculated from hydrodynamic theory determined quantitatively by the usual hydrodynamic parameters. Thus the large quasi-elastic peak (much greater than expected on the basis of hydrodynamic theory) is related to the magnitude of the incoherent scattering. The ratio $\gamma = 0.93$ used for the interpreta-

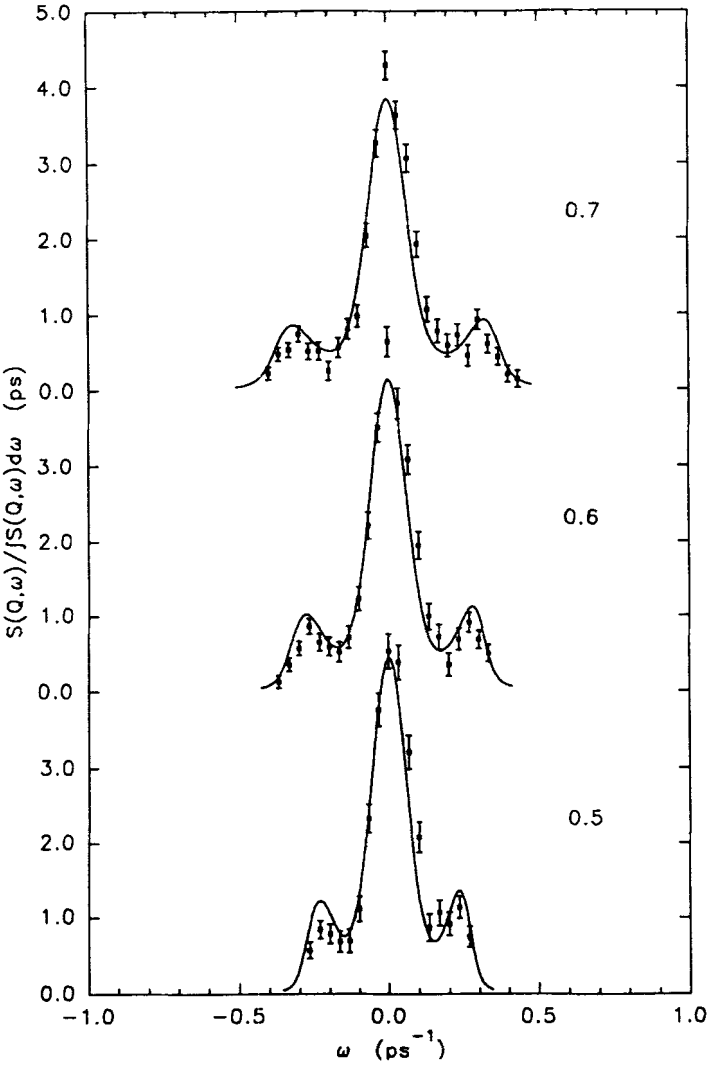

Figure A1 The dynamic structure factor $S(Q,\omega)$ krypton gas at 298 K and 11.5 atoms/nm^3. The numbers on the right hand side are the values of Q in nm^{-1}, and the line is calculated from hydrodynamic theory for the coherent term and from diffusion theory for the incoherent term.

tion of the structure factor, may therefore be tested by theoretical comparisons such as that shown in this figure. If only the ratio γ is varied, the errors shown in the figure allow it to be determined as $\gamma = 0.930 \pm 0.005$. However since other parameters are not known accurately the total error in this measurement of γ is about twice this size.